https://doi.org/10.5194/tc-2023-52
Preprint. Discussion started: 4 May 2023

The Cryosphere Discussions

Calving front monitoring at sub-seasonal resolution: a deep learning application to Greenland glaciers

Erik Loebel[1], Mirko Scheinert[1], Martin Horwath[1], Angelika Humbert[2,3], Julia Sohn[2,4], Konrad Heidler[5], Charlotte Liebezeit[1], and Xiao Xiang Zhu[5]

[1]Technische Universität Dresden, Institut für Planetare Geodäsie, Dresden, Germany
[2]Alfred-Wegener-Institut Helmholtz Zentrum für Polar- und Meeresforschung, Sektion Glaziologie, Bremerhaven, Germany
[3]Universität Bremen, Fachbereich Geowissenschaften, Bremen, Germany
[4]IU Internationale Hochschule, Erfurt, Germany
[5]Technische Universität München, Data Science in Earth Obervation, München, Germany

Correspondence: Erik Loebel (erik.loebel@tu-dresden.de)

Abstract. The mass balance of the Greenland ice sheet is strongly influenced by the dynamics of its outlet glaciers. Therefore, it is of paramount importance to accurately and continuously monitor these glaciers, especially the variation of their frontal positions. A temporally comprehensive parameterization of glacier calving is essential to understand dynamic changes and to constrain ice sheet modelling. However, current calving front records are often limited in temporal resolution as they rely on manual delineation, which is laborious and not feasible with the increasing amount of satellite imagery available. In this contribution, we address this problem by applying an automated method to extract calving fronts from optical satellite imagery. The core of this workflow builds on recent advances in the field of deep learning while taking full advantage of multispectral input information. The performance of the method is evaluated using three independent validation datasets. Eventually, we apply the technique to Landsat-8 imagery. We generate 9243 calving front positions across 23 Greenland outlet glaciers from 2013 to 2021. Resulting time series resolve not only long-term and seasonal signals but also sub-seasonal patterns. We discuss the implications for glaciological studies and present a first application analysing the interaction between calving front variation and bedrock topography. Our method and derived results represent an important step towards the development of intelligent processing strategies for glacier monitoring, opening up new possibilities for studying and modelling the dynamics of Greenland outlet glaciers. Thus, these also contribute to advance the construction of a digital twin of the Greenland ice sheet, which will improve our understanding of its evolution and role within the Earth's climate system.

1 Introduction

Over the past two decades, the Greenland Ice Sheet has been a major contributor to sea level rise (Horwath et al., 2022). Models suggest, that this imbalance will continue with a warming climate (Goelzer et al., 2020; Edwards et al., 2021; Rückamp et al., 2020). About half of the ice mass loss is due to increased meltwater runoff, while the other half is caused by dynamical imbalance (The IMBIE Team, 2020). While changes in the surface mass balance are forced by the atmosphere, the dynamic imbalance is driven by changes at the ice-ocean boundary formed by the outlet glaciers that drain the Greenland Ice Sheet.

https://doi.org/10.5194/tc-2023-52
Preprint. Discussion started: 4 May 2023

Here, several mechanisms act as controls and indicators for dynamic glacier changes. In particular, calving and calving front variations have been identified as crucial parameters for investigating the physical mechanisms of Greenland outlet glaciers (Joughin et al., 2008; Moon and Joughin, 2008; Benn et al., 2017; Trevers et al., 2019; Cook et al., 2021; Melton et al., 2022). In addition, recent studies have shown that calving front retreat is associated with increased ice discharge (King et al., 2018; Mouginot et al., 2019; King et al., 2020). An accurate representation of calving front behaviour is therefore an important requirement for constraining ice sheet modelling and improving simulations of future mass loss and sea level contribution (Vieli and Nick, 2011; Bondizo et al., 2017; Morlighem et al., 2017, 2019). Overall, temporally and spatially comprehensive data products of calving front variation are essential for a better understanding and modelling of marine terminating glaciers.

The steady increase in quality and availability of satellite imagery provides new opportunities for a continuous and accurate monitoring of glacier calving front positions. Nevertheless, current data records mostly rely on manual delineation (Schild and Hamilton, 2013; Joughin et al., 2015; ENVEO, 2017; Andersen et al., 2019; King et al., 2020; Goliber et al., 2022; Black and Joughin, 2023). This is a laborious, time-consuming and therefore ineffective process, given the ever-increasing volume of data. Thus, such calving front products often lack temporal resolution, making seasonal analysis and associated modelling efforts difficult. In response to the need for scalable processing strategies, several empirical feature extraction algorithms have been introduced over the last decades, all aiming to provide robust automated calving front extraction (Sohn and Jezek, 1999; Liu and Jezek, 2004; Seale et al., 2011; Rosenau, 2014; Krieger and Floricioiu, 2017; Liu et al., 2021). Yet, most of these methods are either not tested for spatial transferability and large-scale application, or require case-specific modifications.

With the advent of deep learning and big data methods in remote sensing, new opportunities have emerged to solve complex image processing tasks (Zhu et al., 2017). In recent years, a number of case studies have used deep Artificial Neural Networks (ANN) to extract calving front positions. Both optical (Mohajerani et al., 2019) and synthetic aperture radar (SAR) (Zhang et al., 2019; Baumhoer et al., 2019) sensors have been used. Based on this, numerous studies have advanced the ANN architecture (Heidler et al., 2021; Marochov et al., 2021; Periyasamy et al., 2022; Davari et al., 2022b,a; Heidler et al., 2022), assessed potential input information (Loebel et al., 2022) and pursued the multi-sensor capability (Zhang et al., 2021). In addition, dedicated data products have been developed for training and validation (Goliber et al., 2022) as well as benchmarking (Gourmelon et al., 2022) of ANN applications. Cheng et al. (2021) published the first and only automatically generated data product of calving front locations with a Greenlandic scope.

Building on these achievements, this paper discusses the application and extensive validation of a specially tailored deep learning method for automated calving front extraction using Landsat-8 optical imagery. In doing so, we provide a data product for 23 Greenland outlet glaciers from 2013 to 2021. By exploiting the full multispectral sensor information, we achieve a more accurate and robust calving front extraction compared to using only single band inputs. This significantly increases the temporal resolution of the final product. Thus, the time series of many of the glaciers processed are of unprecedented temporal resolution, resolving their sub-seasonal calving front variability for the first time. By achieving this robust and comprehensive parameterization of glacier calving in Greenland, we meet the glaciology community requirement and make an important first step towards establishing intelligent processing strategies for glacier monitoring tasks. Overall, we provide the

https://doi.org/10.5194/tc-2023-52
Preprint. Discussion started: 4 May 2023

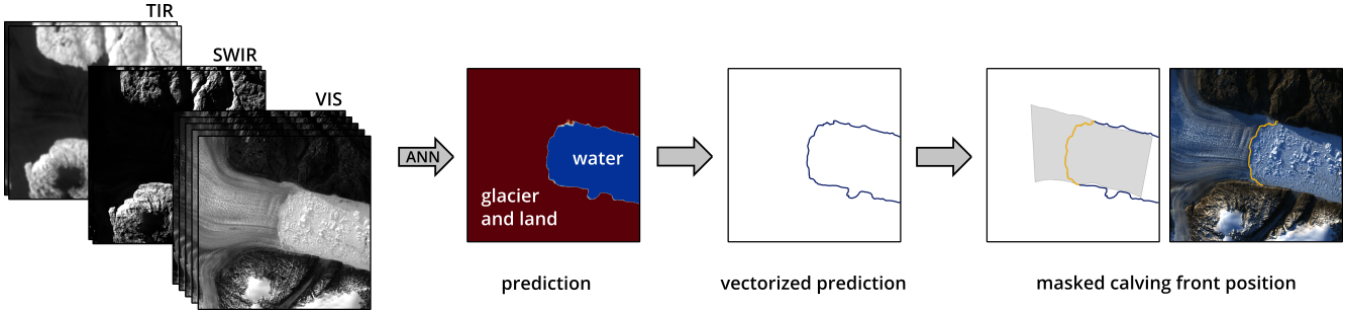

Figure 1. High-level overview of the applied workflow for automated calving front extraction. Based on multispectral satellite imagery in visible (VIS), short-wave infrared (SWIR) and thermal infrared (TIR) wavelengths, the ANN performs a pixel-wise semantic image segmentation. The final calving front position is obtained after vectorizing and masking the ANN prediction. Landsat-8 image courtesy of the U.S. Geological Survey.

wider cryosphere community with a methodology, a data product and implementation as well as a discussion of glaciological implications that open up new possibilities for studying and modelling Greenland glacier dynamics.

Section 2 introduces the applied deep learning method for automated calving front extraction and gives an assessment of its accuracy. In Section 3 we present our data product and the derived time series. As part of the discussion in Section 4, we provide a first application of our results to analyse the interaction between calving front change and bedrock topography. Finally, in Section 5 we draw conclusions and provide an outlook.

2 Delineating calving fronts by deep learning

2.1 Neural network processing

For automated calving front extraction, we apply a modified version of the approach published by Loebel et al. (2022). In doing so, we process multispectral Landsat-8 imagery (Appendix A1) using a specialized ANN (Appendix B). In particular, we use a convolutional neural network of the U-Net architecture (Ronneberger et al., 2015) to semantically segment multispectral imagery into a glacier/land and water class. The glacier calving front, which is described by the boundary between these two classes, is then extracted by vectorizing and masking the model prediction. Figure 1 gives a broad overview of the processing workflow. Larger glaciers, exceeding the fixed window size, are processed by separating the region of interest into multiple independent predictions which are then averaged in the overlapping area prior to vectorization (Baumhoer et al., 2019).

The associated reference data (Appendix A2), which is instrumental both in training and validating machine learning applications, is build from manually delineated calving front positions. To train the ANN model we use 698 calving front locations from 19 Greenland glaciers between 2013 and 2019. As the performance of ANN methods highly depends on training data we pay special attention to cover a diversity of morphological features, different calving and ice mélange conditions as well as varying illumination and cloud situations.

https://doi.org/10.5194/tc-2023-52
Preprint. Discussion started: 4 May 2023

The Cryosphere Discussions
Open Access
EGU

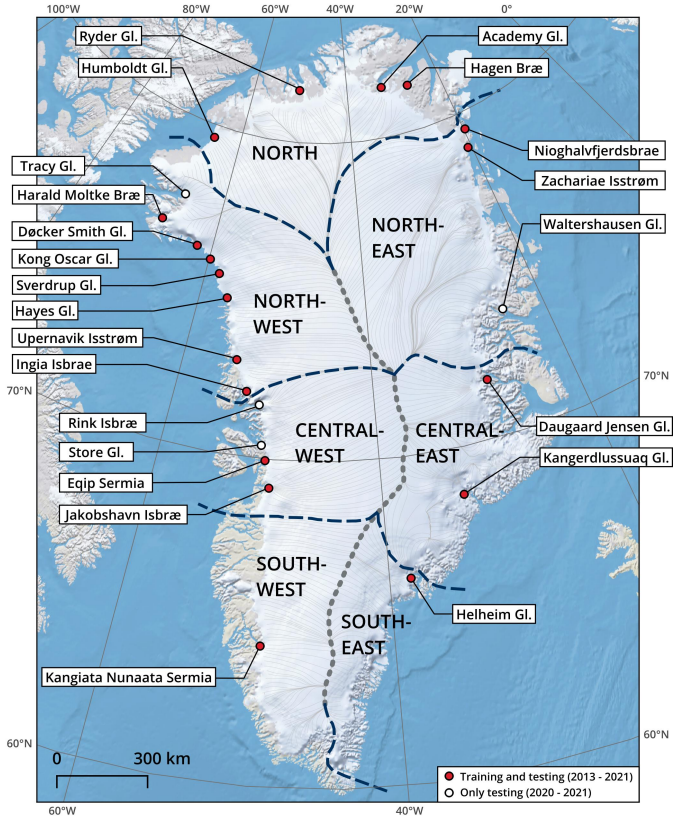

Figure 2. Overview map of the 23 Greenland glaciers used in the TUD reference dataset. Glaciers marked by a red dot are used for training and testing. White dots indicate glaciers only used for model testing. Not on this map: Boydell Glacier, Drygalski Glacier, Storbreen Glacier and Upsala Glacier which are only applied for model testing. The basemap is taken from the QGreenland package (Moon et al., 2022).

2.2 Validation

Our own TU Dresden (TUD) testing set contains 200 labeled images from the years 2020 and 2021. We emphasize that they are temporally separated from the years of the training datasets. To ensure spatial transferability of our method this validation data set includes imagery for additional four Greenland glaciers, two glaciers at the Antarctic Peninsula, one glacier in Svalbard and one glacier in Patagonia. In addition to our own testing dataset we apply another 100 manually picked calving fronts provided by the ESA Greenland Ice Sheet CCI project (ENVEO, 2017) and 110 provided by the CALFIN product (Cheng et al., 2021). Figure 2 gives a spatial overview of the Greenland glaciers used within this study.

The distance between the predicted and the manually delineated calving front is taken as the main error metric in the validation. This is implemented by averaging the minimal distances between the predicted front trajectory and the manual delineation calculated every $30\,\mathrm{m}$. Figure 3 illustrates some validation results for diverse testing images from the three validation

https://doi.org/10.5194/tc-2023-52
Preprint. Discussion started: 4 May 2023

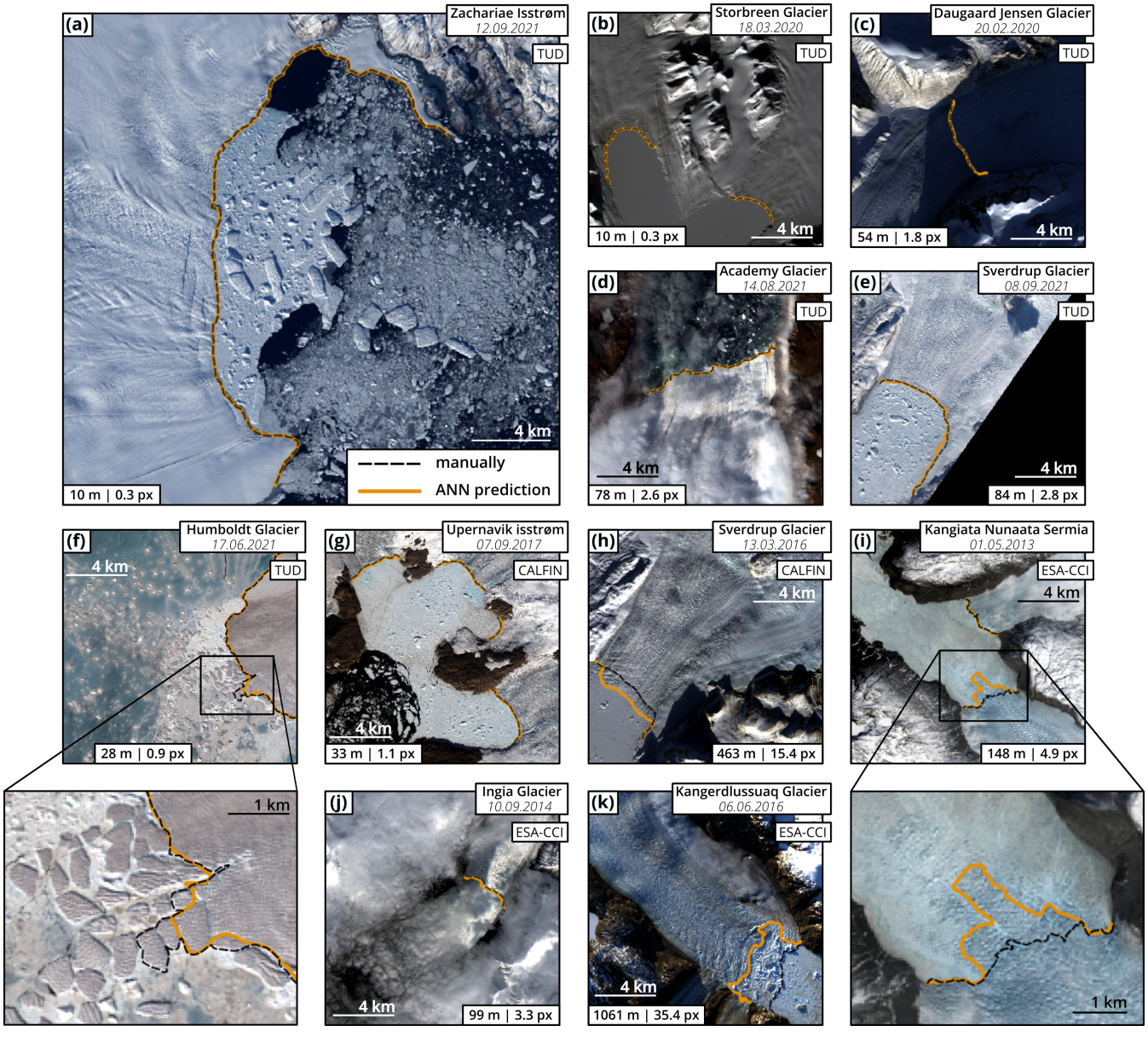

Figure 3. Validation results for example scenes from the (a-f) TUD, (g,h) CALFIN and (i-k) ESA-CCI testing set. Manually delineated calving fronts are depicted as dashed black lines. The ANN prediction is shown in orange. The mean distance error for the respective scene is given both in meters and in pixels. All depicted results derive from the same fitted ANN model. Landsat-8 imagery courtesy of the U.S. Geological Survey.

sets. Along with the manually picked calving front (dashed black) and the ANN delineated calving front (orange) the mean distance between them is indicated. The ANN model reliably delineates calving front locations under a wide range of ocean,

https://doi.org/10.5194/tc-2023-52
Preprint. Discussion started: 4 May 2023

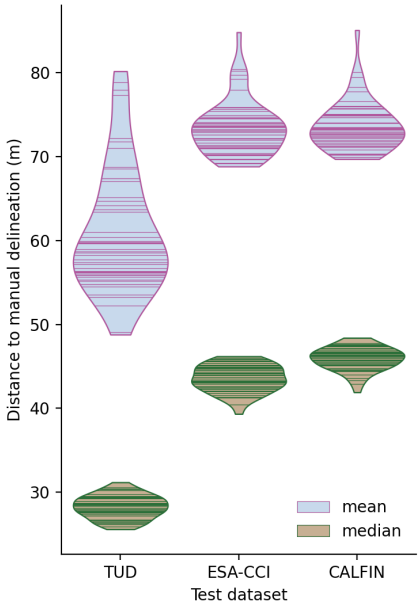

Figure 4. Accuracy assessment for the three independent test datasets. Every horizontal line inside the 'violin graphs' represents one trained model applied to the test dataset. The vertical extent of each graph is defined by the corresponding minimum and maximum values.

sea ice and ice mélange situations. Furthermore, the model is also able to handle images affected by challenging cloud (Fig. 3d, j) and illumination (Fig. 3c) conditions, as well as calving fronts near the edge of a satellite scene (Fig. 3e). Validation images showing large errors are associated to delineation subjectivity (Fig. 3f,h,i) or even human error (Fig. 3k).

Since the ANN training is stochastic every fitted model performs slightly different on our testing data. To ensure statistical stability for a broader numerical assessment we train and validate 50 models using the same reference data and model parameters. In order to assess the distance error, we report both the mean and median over the scenes in the test data set. The validation results for these 50 models are shown in Figure 4. Whereas the mean distance error is sensitive towards outliers the median distance error informs about systematic model overfitting and general scene-by-scene performance. Since each of the three testing data sets originated from its own, hence independent, imagery, resulting error estimates are not directly comparable. Nevertheless, we suspect that the lower distance error yielded for the TUD testing set is due to the fact that it was generated by the same people who inferred the training data for these models. For all three testing sets the ANN mean distance error is below the accuracy level of manual digitization which was estimated by Goliber et al. (2022) to be $107\,\mathrm{m}$ using duplicated delineation from different authors. Altogether, the quality of calving fronts delineated by our ANN model is comparable to that of manually delineated calving fronts.

https://doi.org/10.5194/tc-2023-52
Preprint. Discussion started: 4 May 2023

	Kangiata Nunaata Sermia	Helheim Glacier	Kangerdlussuaq Glacier	Jakobshavn Isbræ	Eqip Sermia	Store Glacier	Rink Isbræ	Daugaard Jensen Glacier	Ingia Isbræ	Upernavik Isstrøm	Waltershausen Glacier	Hayes Glacier	Sverdrup Glacier	Kong Oscar Glacier	Docker Smith Glacier	Harald Moltke Bræ	Tracy Glacier	Humboldt Glacier	Zachariae Isstrøm	Nioghalvfjerdsbræ	Hagen Bræ	Academy Glacier	Ryder Glacier	
2013	5	13	19	15	13	18	20	13	18	6	13	13	14	9	4	16	19	7	15	20	51	54	43	
2014	23	33	42	29	33	40	43	30	30	19	18	33	38	26	25	41	46	32	46	38	66	60	53	
2015	19	24	29	29	32	39	45	26	33	40	25	42	53	44	42	51	58	36	42	40	118	128	100	
2016	17	29	38	26	29	37	44	38	44	33	28	46	48	38	42	51	54	45	60	62	127	127	105	
2017	13	27	39	25	32	36	40	30	41	36	29	40	46	44	38	50	47	38	68	56	126	112	88	
2018	17	17	40	25	35	40	37	29	38	33	39	46	45	34	37	52	54	40	60	50	135	89	114	
2019	15	35	47	34	37	43	46	42	49	46	46	64	60	48	57	54	51	48	73	62	103	99	98	
2020	13	29	40	25	31	35	37	28	47	43	30	40	56	44	53	52	58	47	52	48	93	82	107	
2021	23	31	43	30	29	33	52	56	44	37	41	46	59	48	44	50	49	33	42	64	116	108	86	
Total	145	238	337	238	271	321	364	292	344	293	269	370	419	335	342	417	436	326	458	440	935	859	794	9243

Figure 5. Temporal coverage of our ANN generated time series. The numbers and the color intensity indicate the amount of processed calving front positions in the respective year. Glaciers are sorted by latitude from south (left) to north (right).

3 Results

3.1 Data product for Greenland from 2013 to 2021

Having trained and validated the ANN model, we apply our processing to Landsat-8 imagery in order to generate temporally dense calving front time series for 23 Greenland outlet glaciers. In doing so, we process all but completely clouded Landsat scenes acquired between March 2013 and December 2021. Failed calving front extractions, the percentage of which varies between 5 % and 10 % depending on the glacier, are then manually discarded. Figure 5 gives a tabular overview of the final data product (for locations see Figure 2). In total, we provide 9243 calving front lines, mostly achieving sub-weekly sampling outside polar night. Due to overlapping satellite orbits, glaciers in north, northeast and northwest Greenland undergo up to six image acquisitions per week depending on weather and season. Since we use optical data in this study our time series has observation gaps during polar nights. Depending on latitude, this gap lasts about one month for glaciers in south Greenland and up to three months for glaciers in north Greenland.

3.2 Long term, seasonal and subseasonal calving front changes

Marine terminating glaciers experience calving front variations at different time scales. While long-term changes are easy to resolve using already available data products, our time series offers unique opportunities to analyze seasonal and sub-seasonal terminus changes. To quantify these calving front changes we apply the well-established rectilinear box method (Moon and Joughin, 2008). Rather than using a single profile to measure advance or retreat this method adopts a rectilinear box, thus accounting for uneven changes along the calving front. Figure 6 shows the method applied to our calving front time series for Jakobshavn Isbræ which is separated here into a northern and a southern branch. The inferred calving front variation exhibits a pronounced annual pattern combined with smaller sub-seasonal fluctuations. For comparison, the derived time series of the

https://doi.org/10.5194/tc-2023-52
Preprint. Discussion started: 4 May 2023

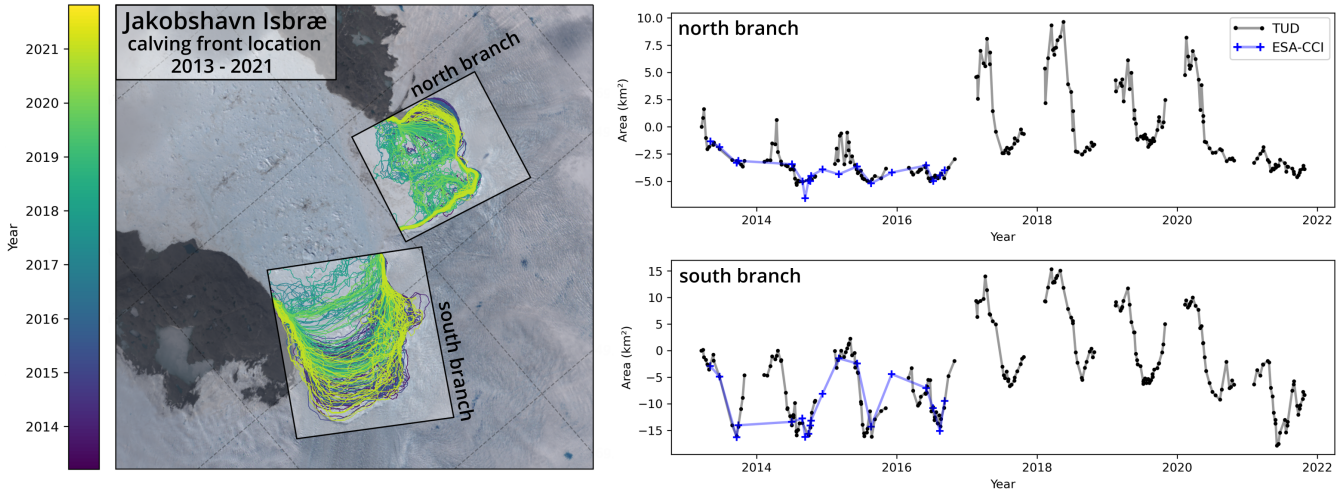

Figure 6. Rectilinear box method applied to the ANN generated calving front time series for Jakobshavn Isbræ (west Greenland). The glacier, which is separated into a northern and a southern branch, and the calving fronts are shown on the left. The corresponding time series are depicted on the right. Here, calving front positions, expressed as a surface area, are marked by a dot. For the TUD product (black) solid lines connect frontal positions of each year. Time series from the ESA-CCI product (blue) are shown for comparison. Landsat-8 image courtesy of the U.S. Geological Survey.

manually delineated ESA CCI product is shown. Although both datasets agree very well when it comes to comparing singular epochs the ESA-CCI time series does not reliably capture the temporal variation. This is particularly evident for the year 2014 when a whole annual cycle is missed by the manually delineated product.

Figure 7 presents twelve more examples of our ANN generated time series. Most of these glaciers exhibit pronounced seasonal and sub-seasonal variations overlaid by a long-term signal. Except for Kangiata Nunaata Sermia (Fig. 7a), Ryder Glacier (Fig. 7b) and Hayes Glacier (Fig. 7h), all example glaciers are retreating during the analysed time period. Notably, Zachariae Isstrøm and Humboldt Glacier show an area loss of about $120\,\mathrm{km}^2$ and $100\,\mathrm{km}^2$ respectively. Ryder Glacier (Fig. 7b) and Nioghalvfjerdsbræ (Fig. 7d) are the only among the 23 glaciers in our study that do not undergo a pronounced seasonality. In those cases, the calving front variation is characterized by a steady advance and the sporadic detachment of large kilometer-sized icebergs. The date of detachment is precisely pinpointed by the time series. In the case of Nioghalvfjerdsbræ (Fig. 7d), the time series also separates two break-offs that occurred in close succession. Other glacier time series, like Hayes Glacier (Fig. 7h), Tracy Glacier (Fig. 7j), Docker Smith Glacier (Fig. 7k) and Harald Moltke Bræ (Fig. 7l), reflect a change in calving rate during our observation period. For Harald Moltke Bræ (Fig. 7l) the onset of this calving front retreat, starting 2019, coincides with the end of its six year-long surging phase and has already been anticipated by Müller et al. (2021).

https://doi.org/10.5194/tc-2023-52
Preprint. Discussion started: 4 May 2023

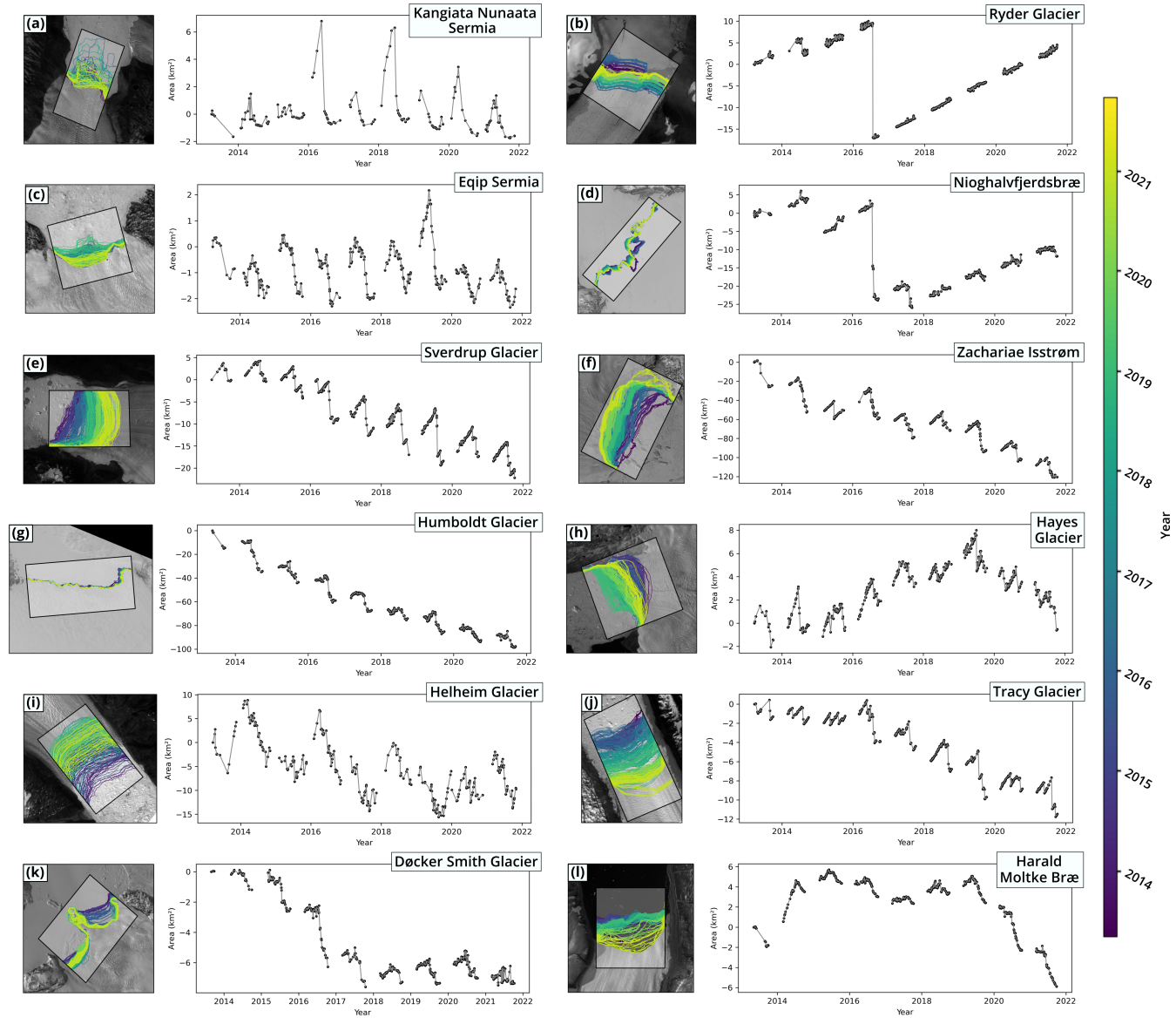

Figure 7. Example time series generated by our ANN algorithm for twelve Greenland glaciers. For each glacier a satellite image (left), containing the color-coded calving front trajectories, and the corresponding time series (right) are shown. Here, calving front positions are marked by black dots and solid lines connecting entries each year. Note that the ordinate axis is scaled differently for each glacier. Landsat-8 imagery courtesy of the U.S. Geological Survey.

https://doi.org/10.5194/tc-2023-52
Preprint. Discussion started: 4 May 2023

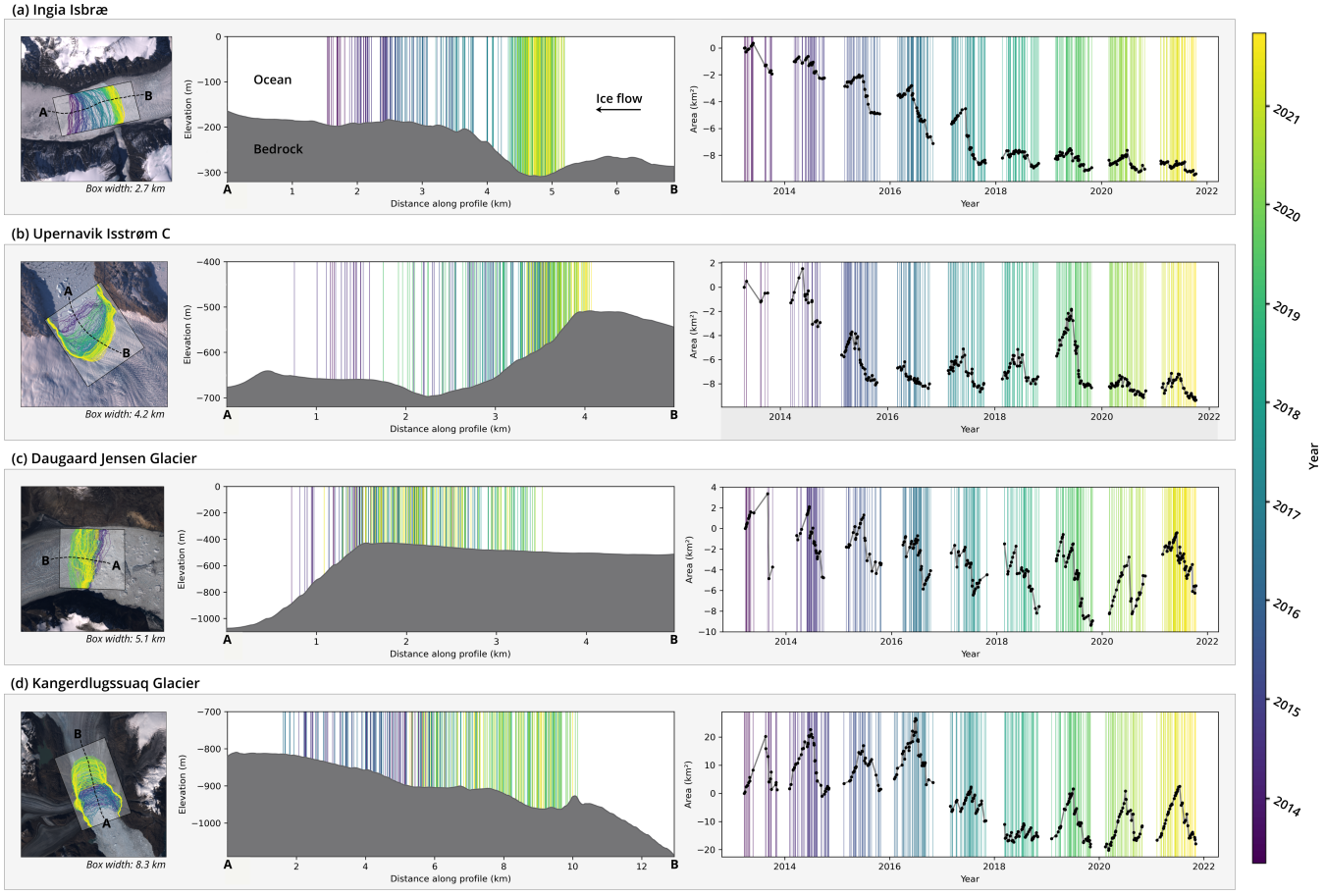

Figure 8. Interaction between calving front variation and bedrock topography for (a) Ingia Isbræ, (b) Upernavik Isstrøm C, (c) Daugaard Jensen Glacier and (d) Kangerdlugssuaq Glacier. Shown are (from left to right) a satellite image with calving front trajectories as well as a marked profile, bedrock topography and color-coded calving front positions along this profile and the corresponding time series of calving front variation. Note that the axis are scaled differently for each glacier. Landsat-8 imagery courtesy of the U.S. Geological Survey.

4 Discussion

Changes in calving front position are, along with other observables like ice velocity and elevation change, part of a complex feedback cycle between a glacier and its environment. In discussing our results, we present a first application of our temporally high-resolution calving front information. In particular, we infer valuable insights into glacier dynamics by linking changes in calving front position to bedrock topography. Figure 8 shows our calving front time series in relation to bedrock elevation, taken from the BedMachine Greenland model (Morlighem, 2022), for four example glaciers. Profiles extend from point A to point B along a central flowline. The calving front of Ingia Isbræ (Fig. 8a) retreated from 2013 to the end of 2017 by 3.2 km (8.6 km^2 in area) with a pronounced seasonal pattern. This retreat is particularly rapid in 2017 and 2018. We suspect this is

https://doi.org/10.5194/tc-2023-52
Preprint. Discussion started: 4 May 2023

due to retrograde topography. Since 2018, the calving front is located in a topographic minimum. This seems to prevent a fast retreat and significantly reduces the seasonal amplitude. In the case of Upernavik Isstrøm C (Fig. 8b), there was a rapid decline in 2014 and 2015, which has slowed considerably since the end of 2015. This is probably a result of the prograde topography of the bedrock. In addition, the seasonal amplitude of the calving front change varies considerably, from a minimum of $1.7\,\mathrm{km}$ ($6.5\,\mathrm{km}^2$ in area) in 2020 to a maximum of $1.7\,\mathrm{km}$ ($6.5\,\mathrm{km}^2$ in area) in 2019. This could be related to the prograde bedrock slope, which leads to a floating and less stable glacier tongue during rapid glacier advance. The calving behavior of Daugaard Jensen Glacier (Fig. 8c) is influenced by the abrupt change of bedrock slope near to the frontal position. An advance beyond this point, from a slightly retrograde into a steeply prograde topography, results in a floating ice tongue. This influences calving behaviour, and in particular results in the calving of large tabular icebergs up to $8.2\,\mathrm{km}^2$ in size. The calving front change of Kangerdlugssuaq Glacier (Fig. 8d) shows high seasonal amplitudes as well as a significant retreat from late 2016 to early 2018. With the exception of 2017 and 2018, where we observe a sustained retreat, the seasonal amplitude remains almost constant at around $4\,\mathrm{km}$ ($21\,\mathrm{km}^2$ in area). Our time series does not show long-term calving front changes since 2018. Considering the bed topography, it is apparent that the glacier front, which was at a stable position until late 2021, has the potential to retreat into a steeply retrograde topography. This retrograde topography continues for about $6\,\mathrm{km}$ upstream. If this tipping point is reached, an accelerated retreat of the glaciers' calving front location might be expected.

These examples further highlight the benefits of the temporally high-resolution calving front information. Long-term calving front trends are often superimposed by seasonal variability and sub-seasonal fluctuations. A separation of these signals is crucial for studying dynamic glacier changes and fully understand underlying processes.

5 Conclusions

This study presents a deep learning based processing system for automatic delineation of calving front locations from multi-spectral Landsat-8 imagery. Using three independent test datasets we validate the performance of our processing system. The quality of the automatically extracted calving fronts is comparable to that of manually delineated calving fronts. By overcoming challenging cloud, illumination and ice mélange conditions we make an important step forward to considerably enhancing both the temporal resolution as well as the coverage of our resulting time series. The time series derived by this processing system resolve long-term, seasonal and sub-seasonal calving front variations. This clearly surpasses the potential of manually delineated data products.

The presented method and the resulting data product addresses the needs of the glaciology community for a comprehensive parameterization of glacier calving in Greenland. The presented example time series highlight the high temporal resolution achieved by our deep learning method. Especially for longer calving fronts, dense sampling is not attainable using manual delineation. Thus, our time series provided for Humboldt Glacier, Zachariae Isstrøm and Nioghalvfjerdsbræ are, among many others, are of unprecedented temporal resolution, resolving their sub-seasonal calving front variability for the first time.

Although the time series presented in this paper give only a selected and a rather narrow glimpse into the dynamics of these glaciers, it is highly important to note that the demonstrated capability of automatically resolving the sub-seasonal calving front

https://doi.org/10.5194/tc-2023-52
Preprint. Discussion started: 4 May 2023

variations is an important step forward towards a spatially comprehensive Greenland wide monitoring system. In conjunction with other components concerning ice flow, elevation change, solid earth response and hydrological processes, this will open up new opportunities to integratively assess, model and simulate dynamic ice sheet changes. Advancing towards this digital twin of the Greenland Ice Sheet will improve our understanding of its evolution and its role within the broader Earth climate system.

Intelligent processing strategies, like deep ANN, will play a major role in shaping the future of glacier monitoring and associated modelling tasks. This is especially true for analyzing the increasing amount of remote sensing imagery. Well-trained and thoroughly validated ANN will be state-of-the-art for automated calving front delineation. The results presented in this paper do not only reinforce existing efforts of deep learning based calving front detection but also lay the foundation for future developments in this field.

https://doi.org/10.5194/tc-2023-52
Preprint. Discussion started: 4 May 2023

Appendix A: Data

A1 Data source

The presented processing system is based on optical Landsat-8 imagery. We use the orthorectified and radiometrically calibrated level 1 data products as provided by the United States Geological Survey (U.S. Geological Survey, 2023). Carrying two scientific instruments, the Operational Land Imager (OLI) and the Thermal Infrared Sensor (TIRS), Landsat-8 provides a particularly wide multispectral coverage. The eleven spectral bands comprise data from visible, near-infrared, short-wave infrared and thermal infrared wavelengths, from $0,435\,\mu\mathrm{m}$ to $1,384\,\mu\mathrm{m}$. With exception to the panchromatic band and the two thermal bands, which have a spatial resolution of $15\,\mathrm{m}$ and $100\,\mathrm{m}$ respectively, all other bands have a resolution of $30\,\mathrm{m}$. Apart from band 9, which is outside an atmospheric window and, therefore, intended for atmospheric observations, all available bands are used as input for our ANN. The integration of these multispectral bands leads to generally more accurate predictions than using conventional single-band inputs only, which has already been shown by Loebel et al. (2022). This is especially true for difficult illumination and ice-melange conditions.

A2 Reference dataset

We use manually delineated calving front locations as reference data. For model training, we use 698 calving front positions across 19 Greenland glaciers between 2013 and 2019. Glaciers are selected for their broad spatial distribution and diverse morphology as well as for different calving and ocean conditions. A spatial overview of all Greenland glaciers applied in this study is given in Figure 2. To test the model we apply three different testing sets. The TUD testing dataset includes four additional Greenland glaciers, Boydell and Drygalski Glacier at the Antarctic Peninsula, Storbreen Glacier in Svalbard as well as Upsala Glacier in Patagonia. In total, the TUD testing set contains 200 calving front positions across 27 glaciers from 2020 and 2021. In addition to our own testing data set we use manually delineated calving fronts from the ESA-CCI (ENVEO, 2017) and the CALFIN (Cheng et al., 2021) product. Here, we use all available calving front positions for our selected Greenland glaciers for which we find a corresponding Landsat-8 scene with less than 24 hours time difference. This results in additional 100 manually delineated calving front positions for the ESA-CCI and 110 for the CALFIN testing datasets.

Appendix B: Methods

B1 Pre-Processing

To use the satellite data as input for the ANN requires pre-processing. In particular, we create stacked raster subsets from the multispectral satellite bands and the manually delineated calving front locations. These subsets have dimensions of $512\,\mathrm{px} \times 512\,\mathrm{px}$ with a unified $30\,\mathrm{m}$ ground sampling distance and are centered on the calving front of the respective glacier. For each multispectral band we apply an image enhancement in form of a cumulative count cut, clipping the data between the 0.1 and 98 percentile, counteracting overexposure in our satellite imagery. Additionally, all satellite bands are then normalized

https://doi.org/10.5194/tc-2023-52
Preprint. Discussion started: 4 May 2023

The Cryosphere
Discussions
Open Access
EGU

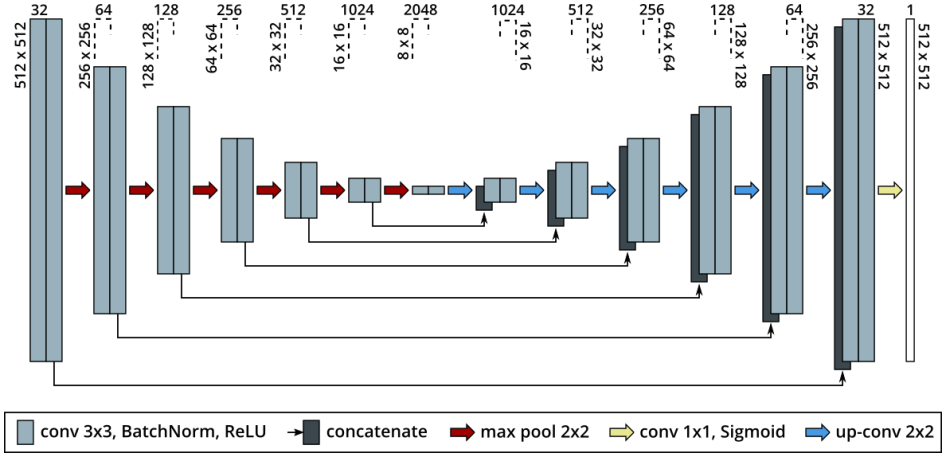

Figure B1. U-Net based model architecture used this study. Contracting sequences are composed of convolutions followed by batch normalization (BatchNorm), a rectified linear unit (ReLU) and a max pooling operation. An expanding sequence is built from a concatenation from the contracting path, convolutions followed by BatchNorm, a ReLU and an up-convolution. The specific dimensions are designated at the top of the blocks.

to the range between 0 and 1 using an 8-bit quantization. Corresponding manually delineated calving front positions, given either as a line string or polygon shape-file, are processed into binary raster masks segmenting land and glacier from ocean. Altogether, one stacked raster subset includes nine satellite bands and a matching ground truth mask.

B2 Semantic image segmentation

To extract the calving front location from the input images we apply a convolutional neural network that performs a pixel-wise semantic image segmentation, separating a glacier-land class from a water class. In particular, we use a U-Net type architecture introduced by Ronneberger et al. (2015). This architecture consists of a contracting path, resembling a typical convolutional network where spatial resolution is reduced while feature information is increased, followed by an expanding path where feature and spatial information are combined. The receptive field of a U-Net is defined by the number of contracting and expanding blocks. As calving front extraction needs adequate spatial context (Heidler et al., 2021) in this study we enhance the U-Net by two additional resolution levels, i.e. from four to six. The applied processing architecture and the relevant dimensions are shown in Figure B1.

Our model is fitted using the pre-processed training data. Before initializing the model training we select every fifth image of the training dataset for internal validation. The remaining training data is augmented eightfold by rotating and flipping. Finally, the resulting 6208 raster subsets are used for fitting the model. For this, we use randomized batches of size eight and apply the Adam optimization algorithm (Kingma and Ba, 2014) on a binary cross-entropy loss function for a total of 200 epochs. Final model weights are selected based on the classification accuracy of the internal validation dataset.

https://doi.org/10.5194/tc-2023-52
Preprint. Discussion started: 4 May 2023

Table C1. Results of the accuracy assessment. The mean and median distance to manual delineation and the confusion matrix for the glacier/land class are given. In addition, the standard deviation of the respective parameters is indicated. Example: Mean TP are all glacier/land image pixels of the test dataset that are correctly classified on average across all 50 models.

Test dataset	Distance to manual delineation		Confusion matrix for the glacier/land class			
	Mean (m)	Median (m)	Mean TP	Mean TN	Mean FP	Mean FN
TUD	61.2 ± 7.5	28.3 ± 1.4	20917160 ± 96881	40922644 ± 39157	701361 ± 96881	85327 ± 39157
ESA-CCI	73.5 ± 3.3	43.6 ± 1.6				
CALFIN	73.7 ± 2.9	45.9 ± 1.4				

The ANN processing is implemented using the TensorFlow 2.4 library (Abadi et al., 2015). Model training is carried out on an IBM Power 9 node and an NVIDIA V100 GPU with 32 GB high bandwidth memory. The training of one model requires about twelve hours with a main memory utilization of 80 GB and an average GPU power consumption of 265 W.

B3 Post-Processing

As output of the ANN output we derive a floating point number probability mask where each image pixel is assigned a probability between 0 (water) and 1 (glacier and land). During post-processing we vectorize this probability mask using the Geospatial Data Abstraction Library (GDAL) contour algorithm (GDAL/OGR contributors, 2020) with a threshold of 0.5. Eventually, we extract the glacier's calving front by intersecting the vectorized coastline trajectory with a static mask. This mask is created manually for each glacier and specifies a corridor of possible calving front locations. Calving fronts exceeding the 512 px $\times$ 512 px window are split into multiple independent predictions which are then averaged in the overlapping area before vectorization. Applying this strategy, which is motivated by Baumhoer et al. (2019), Zachariae Isstrøm, Nioghalvfjerdsbræ and Humboldt Glacier are split into two, three and seven separate overlapping predictions, respectively.

Appendix C: Binary classification metrics

Although our model is fitted using pixel-wise binary cross-entropy the mean and median distances to manual delineation form the main error metric to validate our model. The reason for this is that a high binary classification performance does not necessarily lead to an accurate prediction of the calving front trajectory. The binary classification performance is most important for pixels at the glacier front but less relevant for the rest of the image. Nevertheless, in Table C1 we specify, along with the mean and median distance errors, the confusion matrix of our model accuracy assessment using the TUD test dataset. This confusion matrix enables to derive commonly used binary classification metrics like accuracy, precision, recall or F1-Score making our results more comparable with those of already existing studies.

https://doi.org/10.5194/tc-2023-52
Preprint. Discussion started: 4 May 2023

Code and data availability. The following assets are published along with this article:

- The data product of automatically delineated calving front positions (format: ESRI shapefile), containing 9243 calving front positions across 23 Greenland outlet glaciers, is available at http://dx.doi.org/10.25532/OPARA-208 (Loebel et al., 2023).
- We provide a containerized implementation (platform: Docker) of the presented processing system. The software automatically extracts calving front positions from Landsat-8 or Landsat-9 Level-1 data archives for glaciers used within this study or at user-defined coordinates. This enables the analysis of glaciers that are outside our reference dataset or beyond the temporal frame of our study. The software is available at https://github.com/eloebel/glacier-front-extraction (last access 24 March 2023) and https://doi.org/10.5281/zenodo.7755774 (Loebel, 2023a).
- Our implementation (software: Python 3) of the rectilinear box method is available at https://github.com/eloebel/rectilinear-box-method (last access 24 March 2023) and https://doi.org/10.5281/zenodo.7738605 (Loebel, 2023b).

Author contributions. EL designed the study, developed the methodology, carried out the data processing and time series generation. MS and MH supervised the work and provided direction for the overall study. AH and JS provided key input for the discussion. KH and XXZ contributed to the neural network processing and accuracy assessment. CL assisted in creating the reference dataset. All authors discussed the results and contributed to writing the manuscript.

Competing interests. The author declares that there are no competing interests.

Acknowledgements. We would like to thank the USGS for providing Landsat imagery. Also, we are grateful to the TU Dresden computing centre (ZIH) for providing their high-performance computing and storage infrastructure. We acknowledge the National Snow and Ice Data Center QGreenland package. This work was supported by the Helmholtz Association of German Research Centers as part of the Helmholtz Information and Data Science Incubator, project ”Artificial Intelligence for Cold Regions” (AI-CORE, grant no. ZT-I-0016), and by the German Federal Ministry of Education and Research (BMBF), project "Greenland Ice Sheet/Ocean Interaction" (GROCE2, grant no. 03F0778G).

https://doi.org/10.5194/tc-2023-52
Preprint. Discussion started: 4 May 2023

References

Abadi, M., Agarwal, A., Barham, P., Brevdo, E., Chen, Z., Citro, C., Corrado, G. S., Davis, A., Dean, J., Devin, M., Ghemawat, S., Goodfellow, I., Harp, A., Irving, G., Isard, M., Jia, Y., Jozefowicz, R., Kaiser, L., Kudlur, M., Levenberg, J., Mané, D., Monga, R., Moore, S., Murray, D., Olah, C., Schuster, M., Shlens, J., Steiner, B., Sutskever, I., Talwar, K., Tucker, P., Vanhoucke, V., Vasudevan, V., Viégas, F., Vinyals, O., Warden, P., Wattenberg, M., Wicke, M., Yu, Y., and Zheng, X.: TensorFlow: Large-Scale Machine Learning on Heterogeneous Systems, https://www.tensorflow.org/, software available from tensorflow.org, 2015.

Andersen, J. A., Fausto, R. S., Hansen, K., Box, J. E., Andersen, S. B., Ahlstrøm, A. P., van As, D., Citterio, M., Colgan, W., Karlsson, N. B., Kjeldsen, K. K., Korsgaard, N. J., Larsen, S. H., Mankoff, K. D., Pedersen, A. Ø., Shields, C. L., Solgaard, A., and Vandecrux, B.: Update of annual calving front lines for 47 marine terminating outlet glaciers in Greenland (1999–2018), GEUS Bulletin, 43, https://doi.org/10.34194/GEUSB-201943-02-02, (last access: 11.November 2021), 2019.

Baumhoer, C. A., Dietz, A. J., Kneisel, C., and Kuenzer, C.: Automated Extraction of Antarctic Glacier and Ice Shelf Fronts from Sentinel-1 Imagery Using Deep Learning, Remote Sensing, 11, 2529, https://doi.org/10.3390/rs11212529, 2019.

Benn, D. I., Cowton, T., Todd, J., and Luckman, A.: Glacier Calving in Greenland, Current Climate Change Reports, 3, 282 – 290, https://doi.org/10.1007/s40641-017-0070-1, 2017.

Black, T. E. and Joughin, I.: Weekly to monthly terminus variability of Greenland's marine-terminating outlet glaciers, The Cryosphere, 17, 1–13, https://doi.org/10.5194/tc-17-1-2023, https://tc.copernicus.org/articles/17/1/2023/, 2023.

Bondizo, J. H., Morlighem, M., Seroussi, H., Kleiner, T., Rückamp, M., Mouginot, J., Moon, T., Larour, E. Y., and Humbert, A.: The mechanisms behind Jakobshavn Isbræ's acceleration and mass loss: A 3-D thermomechanical model study, Geophysical Research Letters, 44, 6252–6260, https://doi.org/10.1002/2017GL073309, 2017.

Cheng, D., Hayes, W., Larour, E., Mohajerani, Y., Wood, M., Velicogna, I., and Rignot, E.: Calving Front Machine (CALFIN): Glacial Termini Dataset and Automated Deep Learning Extraction Method for Greenland, 1972–2019 , The Cryosphere, 15, https://doi.org/10.5194/tc-15-1663-2021, 2021.

Cook, S. J., Christoffersen, P., Truffer, M., Chudley, T. R., and Abellán, A.: Calving of a Large Greenlandic Tidewater Glacier has Complex Links to Meltwater Plumes and Mélange, Journal of Geophysical Research: Earth Surface, 126, e2020JF006 051, https://doi.org/https://doi.org/10.1029/2020JF006051, https://agupubs.onlinelibrary.wiley.com/doi/abs/10.1029/2020JF006051, e2020JF006051 2020JF006051, 2021.

Davari, A., Baller, C., Seehaus, T., Braun, M., Maier, A., and Christlein, V.: Pixelwise Distance Regression for Glacier Calving Front Detection and Segmentation, IEEE Transactions on Geoscience and Remote Sensing, 60, 1–10, https://doi.org/10.1109/TGRS.2022.3158591, 2022a.

Davari, A., Islam, S., Seehaus, T., Hartmann, A., Braun, M., Maier, A., and Christlein, V.: On Mathews Correlation Coefficient and Improved Distance Map Loss for Automatic Glacier Calving Front Segmentation in SAR Imagery, IEEE Transactions on Geoscience and Remote Sensing, 60, 1–12, https://doi.org/10.1109/TGRS.2021.3115883, 2022b.

Edwards, T. L., Nowicki, S., Marzeion, B., Hock, R., Goelzer, H., Seroussi, H., Jourdain, N. C., Slater, D. A., Turner, F. E., Smith, C. J., McKenna, C. M., Simon, E., Abe-Ouchi, A., Gregory, J. M., Larour, E., Lipscomb, W. H., Payne, A. J., Shepherd, A., Agosta, C., Alexander, P., Albrecht, T., Anderson, B., Asay-Davis, X., Aschwanden, A., Barthel, A., Bliss, A., Calov, R., Chambers, C., Champollion, N., Choi, Y., Cullather, R., Cuzzone, J., Dumas, C., Felikson, D., Fettweis, X., Fujita, K., Galton-Fenzi, B. K., Gladstone, R., Golledge, N. R., Greve, R., Hattermann, T., Hoffman, M. J., Humbert, A., Huss, M., Huybrechts, P., Immerzeel, W., Kleiner, T., Kraaijenbrink, P.,

Le clec'h, S., Lee, V., Leguy, G. R., Little, C. M., Lowry, D. P., Malles, J.-H., Martin, D. F., Maussion, F., Morlighem, M., O'Neill, J. F., Nias, I., Pattyn, F., Pelle, T., Price, S. F., Quiquet, A., Radić, V., Reese, R., Rounce, D. R., Rückamp, M., Sakai, A., Shafer, C., Schlegel, N.-J., Shannon, S., Smith, R. S., Straneo, F., Sun, S., Tarasov, L., Trusel, L. D., Van Breedam, J., van de Wal, R., van den Broeke, M., Winkelmann, R., Zekollari, H., Zhao, C., Zhang, T., and Zwinger, T.: Projected land ice contributions to twenty-first-century sea level rise, Nature, 593, 74–82, https://doi.org/10.1038/s41586-021-03302-y, 2021.

ENVEO: Greenland Calving Front Dataset, 1990–2016, v3.0, http://products.esa-icesheets-cci.org/products/downloadlist/CFL, (last access: 11.November 2021), 2017.

GDAL/OGR contributors: GDAL/OGR Geospatial Data Abstraction software Library, Open Source Geospatial Foundation, https://gdal.org, 2020.

Goelzer, H., Nowicki, S., Payne, A., Larour, E., Seroussi, H., Lipscomb, W. H., Gregory, J., Abe-Ouchi, A., Shepherd, A., Simon, E., Agosta, C., Alexander, P., Aschwanden, A., Barthel, A., Calov, R., Chambers, C., Choi, Y., Cuzzone, J., Dumas, C., Edwards, T., Felikson, D., Fettweis, X., Golledge, N. R., Greve, R., Humbert, A., Huybrechts, P., Le clec'h, S., Lee, V., Leguy, G., Little, C., Lowry, D. P., Morlighem, M., Nias, I., Quiquet, A., Rückamp, M., Schlegel, N.-J., Slater, D. A., Smith, R. S., Straneo, F., Tarasov, L., van de Wal, R., and van den Broeke, M.: The future sea-level contribution of the Greenland ice sheet: a multi-model ensemble study of ISMIP6, The Cryosphere, 14, 3071–3096, https://doi.org/10.5194/tc-14-3071-2020, https://tc.copernicus.org/articles/14/3071/2020/, 2020.

Goliber, S., Black, T., Catania, G., Lea, J. M., Olsen, H., Cheng, D., Bevan, S., Bjørk, A., Bunce, C., Brough, S., Carr, J. R., Cowton, T., Gardner, A., Fahrner, D., Hill, E., Joughin, I., Korsgaard, N. J., Luckman, A., Moon, T., Murray, T., Sole, A., Wood, M., and Zhang, E.: TermPicks: a century of Greenland glacier terminus data for use in scientific and machine learning applications, The Cryosphere, 16, 3215–3233, https://doi.org/10.5194/tc-16-3215-2022, https://tc.copernicus.org/articles/16/3215/2022/, 2022.

Gourmelon, N., Seehaus, T., Braun, M., Maier, A., and Christlein, V.: Calving fronts and where to find them: a benchmark dataset and methodology for automatic glacier calving front extraction from synthetic aperture radar imagery, Earth System Science Data, 14, 4287–4313, https://doi.org/10.5194/essd-14-4287-2022, https://essd.copernicus.org/articles/14/4287/2022/, 2022.

Heidler, K., Mou, L., Baumhoer, C., Dietz, A., and Zhu, X. X.: HED-UNet: Combined Segmentation and Edge Detection for Monitoring the Antarctic Coastline, IEEE Transactions on Geoscience and Remote Sensing, 2021.

Heidler, K., Mou, L., Loebel, E., Scheinert, M., Lefèvre, S., and Zhu, X. X.: Deep Active Contour Models for Delineating Glacier Calving Fronts, in: IGARSS 2022 - 2022 IEEE International Geoscience and Remote Sensing Symposium, pp. 4490–4493, https://doi.org/10.1109/IGARSS46834.2022.9884819, 2022.

Horwath, M., Gutknecht, B. D., Cazenave, A., Palanisamy, H. K., Marti, F., Marzeion, B., Paul, F., Le Bris, R., Hogg, A. E., Otosaka, I., Shepherd, A., Döll, P., Cáceres, D., Müller Schmied, H., Johannessen, J. A., Nilsen, J. E. Ø., Raj, R. P., Forsberg, R., Sandberg Sørensen, L., Barletta, V. R., Simonsen, S. B., Knudsen, P., Andersen, O. B., Ranndal, H., Rose, S. K., Merchant, C. J., Macintosh, C. R., von Schuckmann, K., Novotny, K., Groh, A., Restano, M., and Benveniste, J.: Global sea-level budget and ocean-mass budget, with a focus on advanced data products and uncertainty characterisation, Earth System Science Data, 14, 411–447, https://doi.org/10.5194/essd-14-411-2022, https://essd.copernicus.org/articles/14/411/2022/, 2022.

Joughin, I., Howat, I., Alley, R. B., Ekstrom, G., Fahnestock, M., Moon, T., Nettles, M., Truffer, M., and Tsai, V. C.: Ice-front variation and tidewater behavior on Helheim and Kangerdlugssuaq Glaciers, Greenland, Journal of Geophysical Research: Earth Surface, 113, https://doi.org/10.1029/2007JF000837, 2008.

Joughin, I., Moon, T., and Black, T.: MEaSUREs Annual Greenland Outlet Glacier Terminus Positions from SAR Mosaics, Version 1, Boulder, Colorado USA. NASA National Snow and Ice Data Center Distributed Active Archive Center, https://doi.org/10.5067/DC0MLBOCL3EL, (last access: 11.November 2021), 2015.

King, M. D., Howat, I. M., Jeong, S., Noh, M. J., Wouters, B., Noël, B., and van den Broeke, M. R.: Seasonal to decadal variability in ice discharge from the Greenland Ice Sheet, The Cryosphere, 12, 3813–3825, https://doi.org/10.5194/tc-12-3813-2018, https://tc.copernicus.org/articles/12/3813/2018/, 2018.

King, M. D., Howat, I. M., Candela, S. G., Noh, M. J., Jeong, S., Noël, B. P., van den Broeke, M. R., Wouters, B., and Negrete, A.: Dynamic ice loss from the Greenland Ice Sheet driven by sustained glacier retreat, Communications Earth & Environment, 1, 1–7, https://doi.org/10.1038/s43247-020-0001-2, 2020.

Kingma, D. P. and Ba, J.: Adam: A Method for Stochastic Optimization, arXiv preprint arXiv:1412.6980, 2014.

Krieger, L. and Floricioiu, D.: Automatic calving front delienation on TerraSAR-X and Sentinel-1 SAR imagery, International Geoscience and Remote Sensing Symposium (IGARSS), https://doi.org/10.1109/IGARSS.2017.8127584, 2017.

Liu, H. and Jezek, K. C.: A Complete High-Resolution Coastline of Antarctica Extracted from Orthorectified Radarsat SAR Imagery, Photogrammetric Engineering and Remote Sensing, 5, 605 – 616, https://doi.org/10.14358/PERS.70.5.605, 2004.

Liu, J., Enderlin, E. M., Marschall, H.-P., and Khalil, A.: Automated Detection of Marine Glacier Calving Fronts Using the 2-D Wavelet Transform Modulus Maxima Segmentation Method, IEEE Transactions on Geoscience and Remote Sensing, 59, 9047 – 9056, https://doi.org/10.1109/TGRS.2021.3053235, 2021.

Loebel, E.: eloebel/glacier-front-extraction: Initial release v1.0.0 [code], Zenodo, https://doi.org/10.5281/zenodo.7755774, 2023a.

Loebel, E.: eloebel/rectilinear-box-method: Initial release v1.0.0 [code], Zenodo, https://doi.org/10.5281/zenodo.7738605, 2023b.

Loebel, E., Scheinert, M., Horwath, M., Heidler, K., Christmann, J., Phan, L. D., Humbert, A., and Zhu, X. X.: Extracting Glacier Calving Fronts by Deep Learning: The Benefit of Multispectral, Topographic, and Textural Input Features, IEEE Transactions on Geoscience and Remote Sensing, 60, 1–12, https://doi.org/10.1109/TGRS.2022.3208454, 2022.

Loebel, E., Scheinert, M., Horwath, M., Humbert, A., Sohn, J., Heidler, K., Liebezeit, C., and Zhu, X. X.: Data product of Greenland glacier calving front locations delineated by deep learning, 2013 to 2021 [data set], TU Dresden OpARA, https://doi.org/http://dx.doi.org/10.25532/OPARA-208, 2023.

Marochov, M., Stokes, C. R., and Carbonneau, P. E.: Image classification of marine-terminating outlet glaciers in Greenland using deep learning methods, The Cryosphere, 15, 5041–5059, https://doi.org/10.5194/tc-15-5041-2021, https://tc.copernicus.org/articles/15/5041/2021/, 2021.

Melton, S. M., Alley, R. B., Anandakrishnan, S., Parizek, B. R., Shahin, M. G., Stearns, L. A., LeWinter, A. L., and Finnegan, D. C.: Meltwater drainage and iceberg calving observed in high-spatiotemporal resolution at Helheim Glacier, Greenland, Journal of Glaciology, p. 1–17, https://doi.org/10.1017/jog.2021.141, 2022.

Mohajerani, Y., Wood, M., Velicogna, I., and Rignot, E.: Detection of Glacier Calving Margins with Convolutional Neural Networks: A Case Study , Remote Sensing, 11, 74, https://doi.org/10.3390/rs11010074, 2019.

Moon, T. and Joughin, I.: Changes in ice front position on Greenland's outlet glaciers from 1992 to 2007, Journal of Geophysical Research: Earth Surface, 113, https://doi.org/10.1029/2007JF000927, 2008.

Moon, T., Fisher, M., Simonoko, H., and Stafford, T.: QGreenland (v2.0.0) [software], https://doi.org/10.5281/zenodo.6369184, https://qgreenland.org, 2022.

Morlighem, M., Williams, C. N., Rignot, E., An, L., Arndt, J. E., Bamber, J. L., Catania, G., Chauché, N., Dowdeswell, J. A., Dorschel, B., Fenty, I., Hogan, K., Howat, I., Hubbard, A., Jakobsson, M., Jordan, T. M., Kjeldsen, K. K., Millan, R., Mayer, L., Mouginot, J., Noël, B. P. Y., O'Cofaigh, C., Palmer, S., Rysgaard, S., Seroussi, H., Siegert, M. J., Slabon, P., Straneo, F., van den Broeke, M. R., Weinrebe, W., Wood, M., and Zinglersen, K. B.: BedMachine v3: Complete Bed Topography and Ocean Bathymetry Mapping of Greenland From Multibeam Echo Sounding Combined With Mass Conservation, Geophysical Research Letters, 44, 11 051 – 11 061, https://doi.org/10.1002/2017GL074954, 2017.

Morlighem, M., Wood, M., Seroussi, H., Choi, Y., and Rignot, E.: Modeling the response of northwest Greenland to enhanced ocean thermal forcing and subglacial discharge, The Cryosphere, 13, 723–734, https://doi.org/10.5194/tc-13-723-2019, https://tc.copernicus.org/articles/13/723/2019/, 2019.

Morlighem, M. e. a.: IceBridge BedMachine Greenland, Version 5, https://doi.org/10.5067/GMEVBWFLWA7X, https://nsidc.org/data/IDBMG4/versions/5, 2022.

Mouginot, J., Rignot, E., Bjørk, A. A., Van den Broeke, M., Millan, R., Morlighem, M., Noël, B., Scheuchl, B., and Wood, M.: Forty-six years of Greenland Ice Sheet mass balance from 1972 to 2018, Proceedings of the national academy of sciences, 116, 9239–9244, 2019.

Müller, L., Horwath, M., Scheinert, M., Mayer, C., Ebermann, B., Floricioiu, D., Krieger, L., Rosenau, R., and Vijay, S.: Surges of Harald Moltke Bræ, north-western Greenland: seasonal modulation and initiation at the terminus, The Cryosphere, 15, 3355 – 3375, https://doi.org/10.5194/tc-15-3355-2021, 2021.

Periyasamy, M., Davari, A., Seehaus, T., Braun, M., Maier, A., and Christlein, V.: How to Get the Most Out of U-Net for Glacier Calving Front Segmentation, IEEE Journal of Selected Topics in Applied Earth Observations and Remote Sensing, 15, 1712–1723, https://doi.org/10.1109/JSTARS.2022.3148033, 2022.

Ronneberger, O., Fischer, P., and Brox, T.: U-Net: Convolutional Networks for Biomedical Image Segmentation, In: Navab N., Hornegger J., Wells W., Frangi A. (eds) Medical Image Computing and Computer-Assisted Intervention – MICCAI 2015., 9351, 234–241, https://doi.org/10.1007/978-3-319-24574-4_28, 2015.

Rosenau, R.: Untersuchung von Fließgeschwindigkeit und Frontlage der großen Ausflussgletscher Grönlands mittels multitemporaler Landsat-Aufnahmen, Ph.D. thesis, Technische Universität Dresden, Qucosa, urn:nbn:de:bsz:14-qucosa-138514, 2014.

Rückamp, M., Goelzer, H., and Humbert, A.: Sensitivity of Greenland ice sheet projections to spatial resolution in higher-order simulations: the Alfred Wegener Institute (AWI) contribution to ISMIP6 Greenland using the Ice-sheet and Sea-level System Model (ISSM), The Cryosphere, 14, 3309–3327, https://doi.org/10.5194/tc-14-3309-2020, https://tc.copernicus.org/articles/14/3309/2020/, 2020.

Schild, K. M. and Hamilton, G. S.: Terminus position time series: Helheim and Kangerdlugssuaq glaciers, Greenland, Arctic Data Center, https://doi.org/10.18739/A2W93G, 2013.

Seale, A., Christoffersen, P., Mugford, R. I., and O'Leary, M.: Ocean forcing of the Greenland Ice Sheet: Calving fronts and patterns of retreat identified by automatic satellite monitoring of eastern outlet glaciers, Journal of Geophysical Research: Earth Surface, 116, https://doi.org/10.1029/2010JF001847, 2011.

Sohn, H. G. and Jezek, K. C.: Mapping ice sheet margins from ERS-1 SAR and SPOT imagery, International Journal of Remote Sensing, 20, 3201 – 3216, https://doi.org/10.1080/014311699211705, 1999.

The IMBIE Team: Mass balance of the Greenland Ice Sheet from 1992 to 2018, Nature, pp. 233 – 239, https://doi.org/10.1038/s41586-019-1855-2, 2020.

https://doi.org/10.5194/tc-2023-52
Preprint. Discussion started: 4 May 2023

Trevers, M., Payne, A. J., Cornford, S. L., and Moon, T.: Buoyant forces promote tidewater glacier iceberg calving through large basal stress concentrations, The Cryosphere, 13, 1877–1887, https://doi.org/10.5194/tc-13-1877-2019, https://tc.copernicus.org/articles/13/1877/2019/, 2019.

U.S. Geological Survey: USGS EarthExplorer, https://earthexplorer.usgs.gov/, (last access: 13.March 2023), 2023.

Vieli, A. and Nick, F. M.: Understanding and Modelling Rapid Dynamic Changes of Tidewater Outlet Glaciers: Issues and Implications, Surveys in Geophysics volume, 32, 437 – 458, https://doi.org/10.1007/s10712-011-9132-4, 2011.

Zhang, E., Liu, L., and Huang, L.: Automatically delineating the calving front of Jakobshavn Isbræ from multitemporal TerraSAR-X images: a deep learning approach, The Cryosphere, 13, 1729–1741, https://doi.org/10.5194/tc-13-1729-2019, 2019.

Zhang, E., Liu, L., Huang, L., and Ng, K. S.: An automated, generalized, deep-learning-based method for delineating the calving fronts of Greenland glaciers from multi-sensor remote sensing imagery, Remote Sensing of Environment, 254, 112 265, https://doi.org/10.1016/j.rse.2020.112265, 2021.

Zhu, X. X., Tuia, D., Mou, L., Xia, G.-S., Zhang, L., Xu, F., and Frauendorfer, F.: Deep Learning in Remote Sensing: A Comprehensive Review and List of Resources, IEEE Geoscience and Remote Sensing Magazine, 5, 8–36, https://doi.org/10.1109/MGRS.2017.2762307, 2017.